Synthesis, Structure, and Acidic Properties of MCM-41 Functionalized with Phosphate and Titanium Phosphate Groups

ARTICLE *in* THE JOURNAL OF PHYSICAL CHEMISTRY B · AUGUST 2005

Impact Factor: 3.3 · DOI: 10.1021/jp0580625 · Source: PubMed

7 AUTHORS, INCLUDING:

T. V. Kovalchuk

12 PUBLICATIONS **111** CITATIONS

SEE PROFILE

Vladimir N. Zaitsev

Pontifícia Universidade Católica do Rio de Ja…

139 PUBLICATIONS **746** CITATIONS

SEE PROFILE

Jacques Fraissard

Pierre and Marie Curie University - Paris 6

243 PUBLICATIONS **3,949** CITATIONS

SEE PROFILE

Synthesis, Structure, and Acidic Properties of MCM-41 Functionalized with Phosphate and Titanium Phosphate Groups

T. V. Kovalchuk,[†] H. Sfihi,[‡,§] A. S. Korchev,[||] A. S. Kovalenko,[†] V. G. Il'in,[⊥] V. N. Zaitsev,[†] and J. Fraissard*[,‡,#,○]

Kiev National T. Shevtchenko University, Chemistry Department, 60, Vladimirskaya str., Kiev 01033 Ukraine, Laboratoire de Physique Quantique, UMR CNRS 7142, ESPCI, 10 rue Vauquelin 75005 Paris, France, Département de Physique UFR SMBH, Université Paris 13, 74 rue Marcel Cochin, 93012 Bobigny, France, Auburn University, Auburn, Alabama, 36849, Institute of Physical Chemistry of L. V. Pisargevskij, National Academy of Science of Ukraine, 31 Prospect Nayki, Kiev, 03039 Ukraine, Laboratoire PMMH, 10 rue Vauquelin, 75005 Paris, France, and Université P. et. M. Curie, 4 Place Jussieu, 75252 Paris Cedex 05, France

Received: February 23, 2005; In Final Form: May 13, 2005

Mesoporous molecular sieves **Si-MCM-41** (purely siliceous) and **Ti-MCM-41** (partly covered with a surface layer of TiO_2) were functionalized with phosphate groups by treatment with $POCl_3$ (denoted **-MCM-41(P)** and **Ti-MCM-41(P)**, respectively). With the use of TEM, X-ray diffraction, and N_2 adsorption, it was shown that the initial hexagonal structure, the high specific surface area, and porosity are retained in the functionalized materials but are not as good as in the starting materials. ^{1}H MAS NMR and ^{31}P MAS NMR revealed that the surface of **Si-MCM-41(P)** consists of silicon phosphate and pyrophosphate species. That of **Ti-MCM-41(P)** additionally contains titanium dihydro-, hydro-, and pyrophosphate species, the latter being predominant. TPD of adsorbed ammonia for **Si-MCM-41(P)** and **Ti-MCM-41(P)** showed that functionalization leads to the creation of moderate and strong acid sites. A combination of mesoporous structure with acidic properties makes the MCM-41 functionalized with phosphate groups promising for use as solid acid catalysts.

1. Introduction

Molecular sieve materials, such as MCM-41 and other ordered silica-based materials, have an organized structure, determined by the orientation of the extended pores: high surface area and narrow pore size distribution.[1] Purely siliceous materials have poor if any catalytic activity. There have been continuous efforts to confer to these materials catalytic activity by introduction of active sites. Thus, inclusion of Al^{3+} ions usually results in an increase in the acidity of the materials, making it similar to that of acidic zeolites.[2] Titanium(IV) ions in siliceous materials can provide active oxidation and photooxidation catalysts.[3] Introduction of Ti^{4+} can be achieved either by their incorporation into the siliceous framework or functionalization of the surface. Unfortunately, the synthetic procedures used for preparation of metallosilicates are often irreproducible, giving rise to materials with unpredictable and variable properties.[4] Moreover, inclusion of Ti^{4+} inside the pore walls of MCM materials is known to substantially worsen their structural order.[5]

The functionalization of the MCM surface can be regarded as an optional method for the creation of active titanium sites.[6] Grafting of titanium species on the surface is usually achieved by treatment with $TiCl_4$. Thus, modification of SBA-materials with $TiCl_4$ yields active epoxidation catalysts.[7] Isolated Ti(IV) sites anchored to the inner pore walls of MCM-41 are of particular significance, as these species were shown to be the catalytically active sites.[8]

We proposed a direct synthesis of mesoporous titanosilicate with a hexagonal siliceous structure and TiO_2 layer localized on the surface of the mesopores.[9] We studied the chemical structure and the acidic properties of the surface species of this material (denoted for the sake of simplicity as **Ti-MCM-41**). Furthermore, we reported the first example of post-functionalization of the resulting materials aiming at the introduction of new catalytic sites. This was possible due to the localization of titanium dioxide on the surface. Interaction of amorphous silica with $POCl_3$ was previously shown to result in the modification of the surface with phosphate groups and formation of acid sites relatively stable to leaching.[10] We used this procedure to functionalize **Ti-MCM-41** and a purely siliceous material (**Si-MCM-41**) with acidic groups in order to develop new solid acids.

In the present article we demonstrate how functionalization via modification with phosphate groups influences the structural characteristics and acidic properties of MCM-type materials.

2. Experimental SectionTechniques

2.1. Sample Preparation and Elemental Analysis. Titanium tetrabutoxide (TBOT) (Angarsk) was used as the titanium precursor. The silicon precursor, sodium silicate, was prepared by dissolution of highly dispersed silica (Aerosyl-300, Oriana, Kalush) in aqueous sodium hydroxide.[11] Myristyltrimethylammonium bromide (MTMAB) (Fluka) was used as surfactant. The composition of the initial reaction mixture (mol) was as

* Corresponding author. E-mail: jfr@ccr.jussieu.fr.
† Kiev National T. Shevtchenko University.
‡ Laboratoire de Physique Quantique, UMR CNRS 7142, ESPCI.
§ Université Paris 13.
|| Auburn University.
⊥ National Academy of Science of Ukraine.
Laboratoire PMMH.
○ Université P. et. M. Curie.

10.1021/jp0580625 CCC: $30.25
Published on Web 06/29/2005

TABLE 1: P, Ti, and H_2O Content in Si-MCM-41(P) and Ti-MCM-41(P) Samples

samples	TiO_2 (wt %)	Ti (mmol g^{-1})	PO_4 (wt %)	P (mmol g^{-1})	H_2O (wt %)
Si-MCM-41(P)			9.6	1.0	25
Ti-MCM-41(P)	9.1	2.2	20.7	2.2	15.5

follows: xTBOT:SiO_2:0.33Na_2O:0.20MTMAB:400H_2O:x(*i*-PrOH), where x was 0.160.

The starting **Si-MCM-41** and **Ti-MCM-41** (TiO_2 content 10.5 mol %) were prepared according to the work of Kovalenko et al.[9] To an aqueous solution of MTMAB were added a 1:1 mixture of TBOT with *i*-PrOH and an aqueous solution of sodium silicate with vigorous stirring. The suspension obtained was magnetically stirred at ambient temperature for 10−12 h and kept without agitation for another 10−12 h. The resulting precipitate was filtered off, washed with distilled water and dried in air at 100 °C (as-synthesized sample). The samples were subjected to hydrothermal treatment at 100 °C for 3 days, filtered off, washed with distilled water, and dried in air at 100 °C. Finally, they were calcined at 540 °C for 4 h to remove the template.

Samples **Si-MCM-41(P)** and **Ti-MCM-41(P)** were prepared as follows. The precursors, **Si-MCM-41** and **Ti-MCM-41**, were treated with $POCl_3$ in anhydrous toluene for 5 h at 70 °C with vigorous stirring, as in ref 10. The solid was filtered off, washed with toluene and dried for 2 h at 100 °C. The samples were treated with steam at 180 °C for 2 h to hydrolyze residual P−Cl bonds, and dried at 180 °C. The results of elemental analysis are given in Table 1.

2.2. Physical and Chemical Analysis. *2.2.1. Thermal Analysis.* Thermal analysis, including thermoprogrammed desorption (TPD), differential thermal analysis (DTA), differential thermogravimetric (DTG), and thermogravimetric (TG) measurements**,** was performed using a MOM Q-1000 derivatograph (temperature gradient 10 °C/min) against alumina as standard.

2.2.2. Nitrogen Adsorption Isotherms. The nitrogen adsorption isotherms were measured on ASAP 2010 Micromeritics equipment after preliminary treatment of the samples under vacuum at 150 °C for 15 h. Specific surface areas were calculated according to the BET equation. Pore size distribution and pore volume were determined from the isotherm desorption branch by the Kelvin equation (BJH formula) using the cylindrical pore approximation.

2.2.3. Acidity Measurements. Sample acidity was studied by measuring the TPD of preadsorbed ammonia. The samples were activated at 200 °C (or, optionally, at 450 °C) for 1 h under N_2 flow and cooled to 100 °C. After saturation in NH_3 flow at 100 °C, the physically adsorbed ammonia was desorbed by N_2 flow for 1 h at 100 °C. Residual ammonia was desorbed by continuous heating to 450 °C in N_2 flow at 17 °C/min. The amount of desorbed ammonia was measured by gas chromatography and titration with HCl.

2.2.4. TEM. Transmission electronic microscopy (TEM) images were obtained with a JEOL JEM 100CXII microscope.

2.2.5. XRD. Powder X-ray diffractograms (XRD patterns) were recorded in the scan range of 2θ between 1.5 and 20° using Cu/Ni 30 kV/20 mA radiation (Cu Kα, $\lambda = 1.54178$ Å) on a DRON-3M X-ray diffractometer. Silicon and quartz were used as internal standards.

2.2.6. NMR. ^1H and ^{31}P single pulse excitation (SPE) and magic angle spinning (MAS) nuclear magnetic resonance (NMR) measurements were made at 400.13 and 202.46 MHz, respectively, with Bruker MSL 400 and ASX 500 spectrometers, respectively.

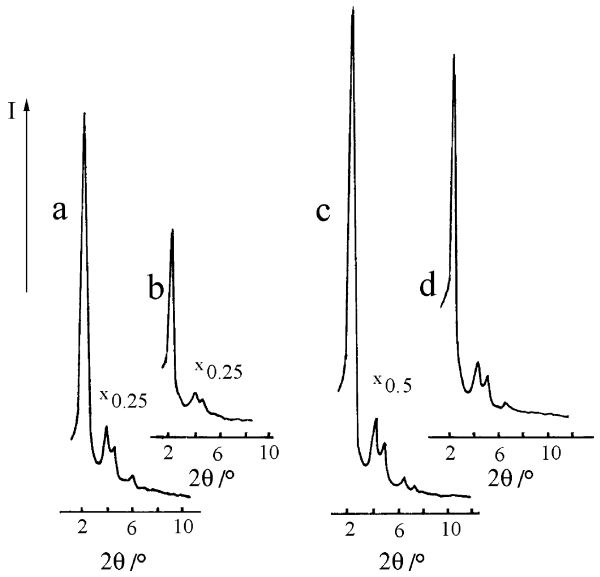

Figure 1. X-ray diffractograms of (a) **Si-MCM-41**, (b) **Si-MCM-41-(P)**, (c) **Ti-MCM-41**, and (d) **Ti-MCM-41(P)**.

For ^1H SPE-MAS measurements, the samples were treated at 0.02 Pa at 130 °C for 24 h and sealed in 7 mm glass tubes. With such tubes, the spinning frequency was 2−3 kHz. The number of accumulations was typically 64 and the delay between each accumulation was 10 s in accordance with the ^1H spin lattice relaxation times.

To distinguish between the chemically and physically bound phosphates, the ^{31}P NMR measurements were recorded under MAS (SPE-MAS) and static (SPE) conditions. The sample powder was filled into a 4 mm zirconia rotor and spun at 7 kHz in SPE-MAS measurements. The number of accumulations was 32 and the delay between each accumulation was 30 s in accordance with the ^{31}P spin lattice relaxation times.

The ^1H and ^{31}P chemical shifts were referenced to external standards of tetramethylsilane (TMS) and 85% H_3PO_4, respectively.

Both ^1H and ^{31}P NMR experimental spectra were fitted using a mixture of Gaussian and Lorentzian lines. The contribution of each line to the whole intensity of the fitted spectrum was determined by taking into account the intensity of the spinning sidebands.

2.2.7. FTIR. Fourier transform infrared (FTIR) spectra of the samples were obtained in the transmission mode for 1:4 KBr diluted samples pressed into pellets, on a Bruker Vector 22 spectrometer. The spectral resolution was 4 cm^{-1} and the number of scans 200. The samples were preactivated by 0.2 Pa vacuum treatment at 150 °C for 1 h, but exposed to air during the measurements.

3. Results

3.1. Physical Characteristics. According to the XRD analysis (Figure 1), both **Si-MCM-41(P)** and **Ti-MCM-41(P)** preserve the ordered hexagonal structure of the initial materials and consists of a single phase.[2] Moreover, X-ray diffractograms of a starting **Ti-MCM-41** and resulting **Ti-MCM-41(P)** (recorded up to $2\theta = 20°$) show the absence of the crystalline anatase phase.

The modification with phosphate groups considerably reduces the intensities of the XRD peaks: 2- and 2.7-fold for **Si-MCM-41(P)** and **Ti-MCM-41(P)**, respectively. However, the lattice parameters (a_o) are not affected by functionalization. The

TABLE 2: Textural Characteristics of MCM Samples, According to X-ray Analysis and to N_2 Adsorption Isotherms[a]

parameters	Si-MCM-41	Si-MCM-41(P)	Ti-MCM-41	Ti-MCM-41(P)
S_{BET}, $m^2\ g^{-1}$	1132	819	848	510
V, $cm^3\ g^{-1}$	0.949	0.595	0.605	0.221
D, Å	25.6	24.2	22.6	18.4
a_o, Å	43.4	43.4	40.8	40.8
d_{100}, Å	37.6	37.6	35.3	35.3
W, Å	17.8	19.2	18.2	22.4

[a] S_{BET} is the specific surface area, V the total pore volume, D the mean pore diameter, a_o the lattice parameter, d_{100} the interplanar distance. Parameter W is calculated as $a_0 - D$.

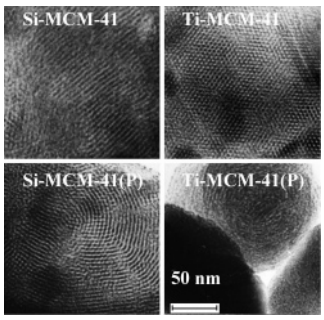

Figure 2. TEM images of the starting MCM-41 samples and their phosphorylated derivatives.

calculated a_o values (Table 2) are 43.4 and 40.8 Å for **Si-MCM-41(P)** and **Ti-MCM-41(P)**, respectively.

The TEM images (Figure 2) show that the phosphorylated materials conserve the ordered hexagonal structure of the starting materials (**Si-MCM-41** and **Ti-MCM-41**), though they are slightly amorphized, especially sample **Ti-MCM-41(P)**. The presence of a small amount of amorphous phase observed in the TEM images of both **Si-MCM-41(P)** and **Ti-MCM-41(P)** may be due to the formation of an amorphous silicon and titanium phosphate.

Nitrogen adsorption on functionalized and starting solids is described by IV-type isotherms (IUPAC), which is typical for MCM-41 (Figure 3). The isotherms are characterized by a sharp inflection at $P/P° \sim 0.4$, resulting from condensation in the mesopores. Only an insignificant hysteresis loop is observed at $P/P° = 0.9$. The BET surface areas (N_2 adsorption) of **Ti-MCM-41** and of **Si-MCM-41** decrease after modification with phosphate groups by 338 and 313 $m^2\ g^{-1}$, respectively (Table 2).

The pore size distribution of the samples after modification with phosphate groups (Figure 4) is characterized by small half-widths (ca. 3−4 Å), indicating that the molecular sieve properties of the materials are retained. The values of the mean pore diameter calculated for the different samples are given in Table 2. It can be seen that the mean pore diameter of **Ti-MCM-41** (22.6 Å) is smaller than that of **Si-MCM-41** (25.6 Å). This is associated with the TiO_2 layer on the walls of the mesopores. Phosphate modification of both samples results in a slight reduction of the mean pore diameter for **Si-MCM-41(P)** (24.2 Å), and a much greater reduction for **Ti-MCM-41(P)** (18.4 Å). Furthermore, the pore volumes of the phosphated samples decrease significantly. Indeed, the pore volumes decrease from 0.948 to 0.595 and from 0.605 to 0.221 $cm^3\ g^{-1}$ for **Si-MCM-41(P)** and **Ti-MCM-41(P)**, respectively. This is related to the wall-grafted phosphate groups that are present in high concentration in the samples (1.0 mmol g^{-1} in **Si-MCM-41(P)** and 2.2 mmol g^{-1} in **Ti-MCM-41(P)**).

The difference, W, between the pore diameter, D, and the hexagonal cell parameter, a_o, is increased by the deposition of phosphate moieties from 17.8 to 19.2 and from 18.2 to 22.4 Å

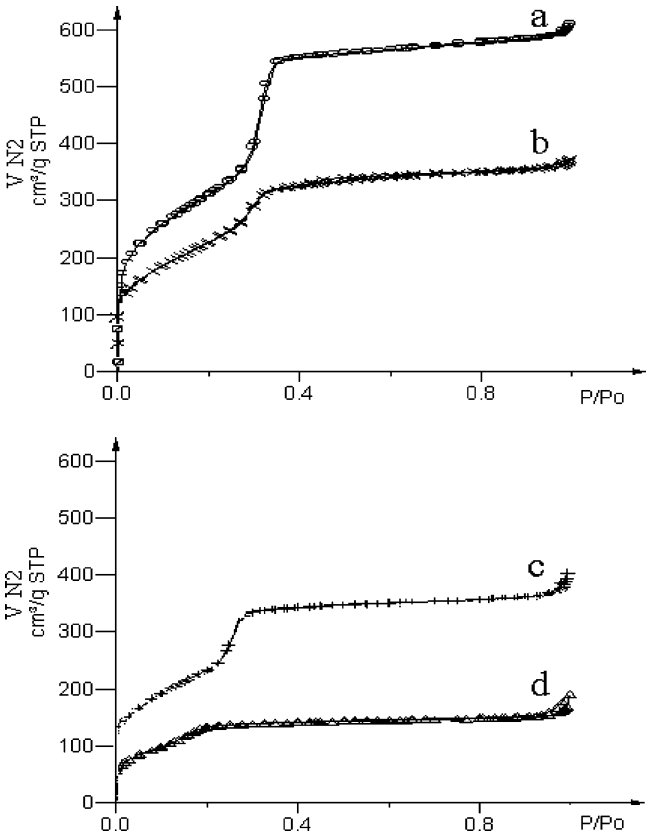

Figure 3. N_2 adsorption/desorption isotherms of (a) **Si-MCM-41**, (b) **Si-MCM-41 (P)**, (c) **Ti-MCM-41**, and (d) **Ti-MCM-41(P).**

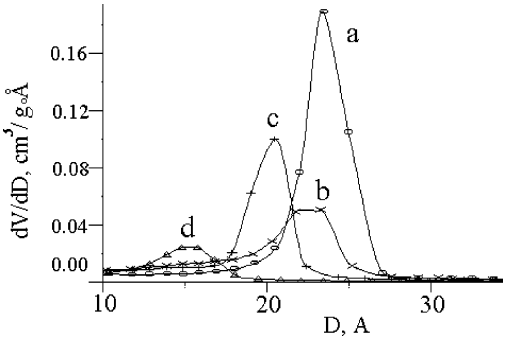

Figure 4. Pore size distribution profile (desorption branch) of (a) **Si-MCM-41**, (b) **Si-MCM-41 (P)**, (c) **Ti-MCM-41**, and (d) **Ti-MCM-41(P)**.

for **Si-MCM-41(P)** and **Ti-MCM-41(P)**, respectively (Table 2). W corresponds to the wall thickness plus the thickness of the chemisorbed phosphate layer. However, the d_{100} values (Table 2) are not changed by the modification, which suggests comparable pore wall thickness: $d_{100} = 37.6$ Å for **Si-MCM-41** and **Si-MCM-41(P)** and 35.3 Å for **Ti-MCM-41** and **Ti-MCM-41(P)**, respectively (Table 2).

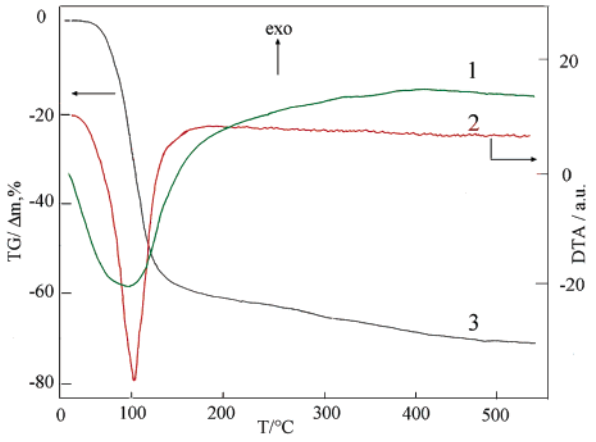

Figure 5. Thermal analysis of **Ti-MCM-41(P)** including (1) differential thermal analysis (DTA), (2) differential thermogravimetric curve (DTG), and (3) thermogravimetric curve (TG).

3.2. Thermogravimetry. The results of the thermogravimetric study of **Ti-MCM-41(P)** are presented in Figure 5. The DTG curve (Figure 5-2) shows that **Ti-MCM-41(P)** begins to lose weight at 40 °C. This loss, which is related to the loss of adsorbed water and represents 18% of the initial weight, is accompanied by an endothermic effect with a maximum at 105 °C, as shown by the DTA curve (Figure 5-1). The TG curve (Figure 5-3) indicates that the weight loss is initially fast and becomes slower in the 140−170 °C range. Further increase of temperature causes a slow linear reduction of the sample weight without any appreciable exothermic effect. Up to 560 °C the total weight loss is ca. 26% (Figure 5-3). The loss at these temperatures (170−560 °C) is probably due to dehydration of the grafted silicon and titanium phosphates (the chemical nature of these species is established by spectroscopic characterization). In addition, dehydroxylation of the surface (condensation of ≡Si−OH and ≡Ti−OH groups) occurs at high temperatures.

It is known that orthophosphoric acid loses one molecule of water and turns into pyrophosphoric acid at 260 °C.[12] Upon further heating to 300 °C, it loses a second molecule of water and becomes polymeric metaphosphonic acid $(HPO_3)_n$. These two processes are exothermic (17 and 24 kcal mol^{-1}, respectively, for the processes mentioned).[12] If it is assumed that the dehydration of the immobilized acid proceeds in a similar way, one water molecule can be lost per immobilized acid. Since the contribution of dehydroxylation to the total weight loss at 260−400 °C is relatively small, the concentration of immobilized acid (from the weight loss) can be estimated as 1.5 mmol g^{-1}. However, a greater value for the phosphate group concentration (2.2 mmol g^{-1}) was obtained from the elemental analysis data (Table 1). Therefore, it can be suggested that not all the bonded phosphate groups contain acidic hydrogens able to condense and release water (as assumed, for example, for titanium pyrophosphate). The absence of any noticeable exothermic effect on the differential thermal analysis curve (Figure 5-1) corresponding to the dehydration of phosphoric acid can be explained by its slowness.

The TG, DTG, and DTA curves for **Si-MCM-41(P)** are similar to those of **Ti-MCM-41(P)**, so they are not given here. Heating **Si-MCM-41(P)** results in a weight loss of 15%, with a maximum at 105 °C, and the total loss is 21%. As with sample **Ti-MCM-41(P)**, the weight loss in the interval 260−400 °C can be used to estimate the concentration of the grafted phosphoric acid. The calculated value, 1.3 mmol g^{-1}, correlates with the concentration of the phosphate group, obtained from elemental analysis (1.0 mmol g^{-1}). The similarity of these two values suggests that, in contrast to **Ti-MCM-41(P)**, all the phosphate groups bonded to the surface of **Si-MCM-41(P)** contain hydrogens.

3.3. Spectroscopy. *3.3.1. ^1H SPE- MAS NMR.* The ^1H SPE-MAS NMR spectra of the different samples are shown in Figure 6. The ^1H NMR spectra of several types of TiO_2 and titanium-containing silica are reported to depend markedly on the synthesis procedure and the dehydration temperature.[13,14] For titanium-containing silica, whatever the preparation and physical properties, two peaks are generally observed at ca. 2.3 and 6.4 ppm, which are further decomposed into several overlapping lines. The peak at 2.3 ppm is attributed to the nonacidic protons of ≡Ti−OH groups. That at 6.4 ppm is attributed to acidic protons of bridged ≡Si−(OH)−Ti≡ groups. ^1H NMR spectra of phosphate-containing silica, depending on the phosphate concentration and treatment temperature, are reported to display, besides a resonance at 1.9 ppm attributed to ≡SiOH, additional peaks at 3.5, 8.8, and 10.7 ppm.[14] or 8.5−9.5 ppm.[16] By analogy with the spectra of polycrystalline SiP_2O_7 and $Si(HPO_4)_2$, which display peaks at 3.5 and 10.7 ppm, respectively, these peaks are attributed to the P−OH groups of the grafted acid.[14]

Si-MCM-41. The ^1H SPE-MAS NMR spectrum of **Si-MCM-41** (Figure 6a, Table 3) contains a single narrow peak at 1.8 ppm corresponding to isolated ≡SiOH. In the NMR spectra reported for amorphous silica, this peak is located at 1.7 ppm.[14,15] The peak observed here contains a very weak downfield shoulder. This shoulder is particularly visible in the spinning sidebands, indicating that the ^1H chemical shift anisotropy of the corresponding species is greater than that of isolated ≡SiOH (1.8 ppm). These species are the vicinal silanols and the silanols forming hydrogen bonds with water, ≡Si−OH···H_2O, which were reported to resonate at 2.4 and 3.5 ppm, respectively (Table 3). The peaks corresponding to these species were correctly fitted by a mixture of Gaussian and Lorentzian lines. However, the relative amount of these two species remains very small (Table 3).

Ti-MCM-41. In addition to the main peak at 1.8 ppm attributed to isolated silanols, the SPE-MAS spectrum of **Ti-MCM-41** (Figure 6c) exhibits a new resolved peak, at 6.9 ppm, ascribed to the bridged acidic protons of ≡Si−(OH)−Ti≡. The whole spectrum was correctly fitted by a mixture of Gaussian and Lorentzian lines. The NMR characteristics of these fitted lines and their assignments are given in Table 3. This fit was done by taking into account the reference data on the NMR spectra of titanium-containing silica materials and by assuming the existence of the above-mentioned groups on the surface of **Ti-MCM-41**.[13,14] The peak at 1.8 ppm is broader and more asymmetric than that observed for **Si-MCM-41** (Figure 6a). This reflects an important contribution of protons due to ≡Ti−OH. The peak at 2.4 ppm might arise from the superposition of the signals of ≡Ti−OH and the vicinal ≡Si−OH groups,[14] and that at 3.4 ppm is tentatively attributed to the ≡Si−OH and ≡Ti−OH groups hydrogen-bonded to water.

Si-MCM-41(P). Similar to that of **Si-MCM-41**, the ^1H SPE MAS spectrum of **Si-MCM-41(P)** (Figure 6b) also contains a peak at 1.8 ppm but with a stronger downfield shoulder. Assuming the existence of hydroxyl and phosphate species, [14] the shoulder was fitted by two lines at 2.6 and 3.5 ppm (Table 3). They are assigned to vicinal silanols ≡Si−OH···≡Si−OH and to the P−OH group of the immobilized acid in the surface analogues of silicon pyrophosphate structures, respectively. However, we do not exclude a contribution to the intensity of the shoulder by water hydrogen-bonded to silanols, which displays a peak at 3.5 ppm.

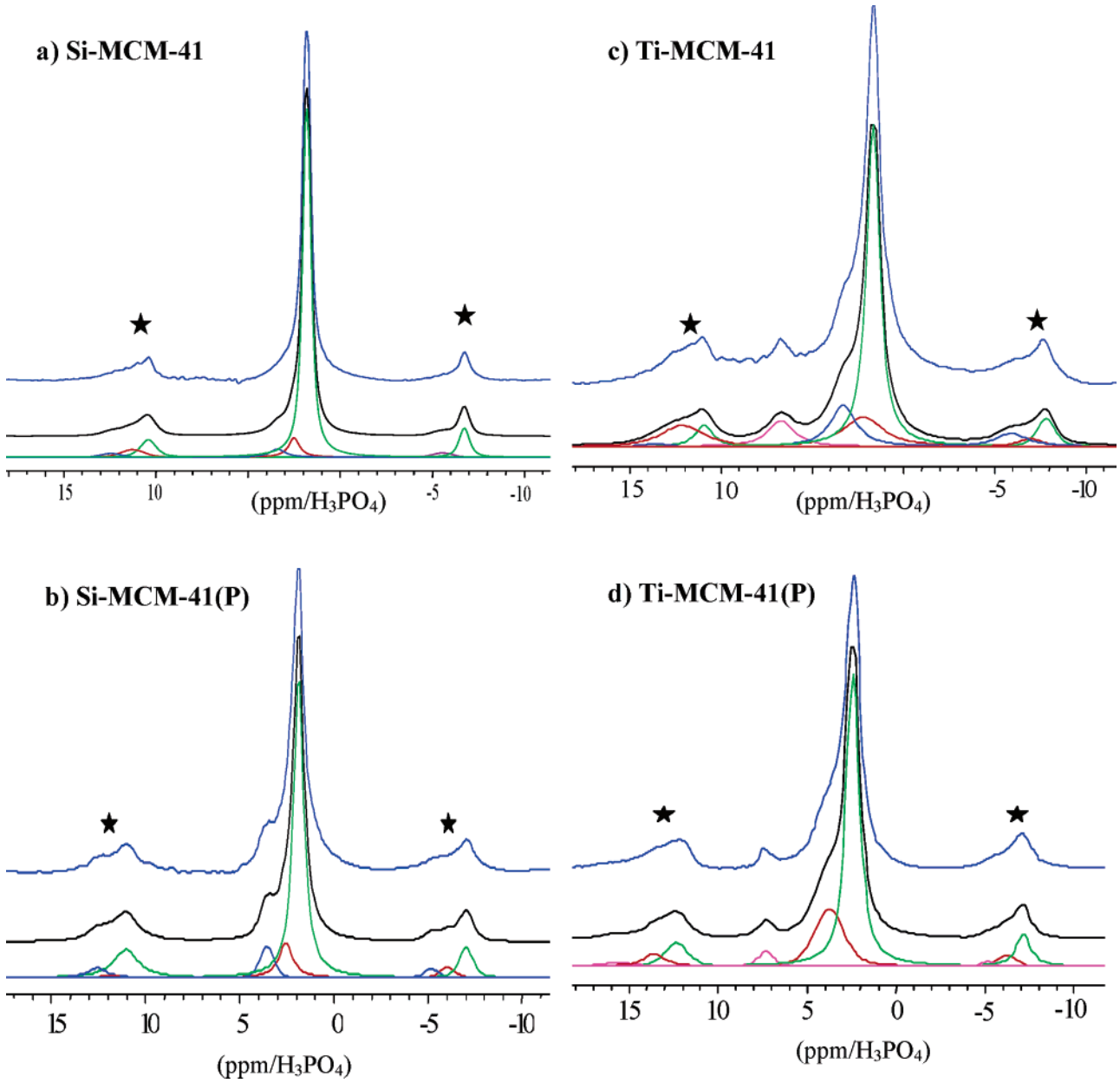

Figure 6. Top to bottom: ^{1}H SPE-MAS NMR spectra of MCM samples, sum of the fitted lines, and each fitted line. (∗) spinning sidebands.

TABLE 3: Characteristics and Assignment of the Fitted Lines of the ^{1}H SPE-MAS NMR Spectra of Samples

samples	position (ppm)	rel inten (%)	width at half maximum (Hz)	assignment
	1.8	89	200	≡SiOH isolated
Si-MCM-41	2.4	5	300	≡SiOH vicinal
	3.5	6	900	≡SiOH...H_2O
	1.8	74	300	≡SiOH isolated
Si-MCM-41(P)	2.6	10	250	≡SiOH vicinal
	3.5	16	550	≡SiO−PO(OX)-$PO(OX)_2$, X = H, Si≡ ≡SiOH···H_2O (residual)
	1.8	71	350	≡SiOH isolated
Ti-MCM-41	2.4	12	1000	≡TiOH isolated, ≡SiOH vicinal
	3.5	12	650	≡SiOH···H_2O; ≡TiOH···H_2O
	6.9	5	700	≡Ti(OH)Si≡
	2.1	76	350	≡SiOH, ≡TiOH (isolated, vicinal)
Ti-MCM-41(P)	3.4	18	750	≡SiOH···H_2O (residual), ≡TiO−$PO(OH)_2$, ≡SiO−PO(OX)-$Si(OX)_2$, X = H, Si≡
	6.9	6	350	≡Ti(OH)Si≡

The absence of the peak at ca. 10.7 ppm corresponding to more acidic protons of $Si(HPO_4)_2$ may be due to the acid concentration in the sample studied (9.6 wt %, Table 1) being somewhat low, compared to that reported in reference.[14] This peak may also be hidden by overlap with the spinning sidebands. However, on the basis of the structure of the upfield spinning sideband (−5/−9 ppm) which is similar to that appearing downfield (9/14 ppm), it can be suggested that a peak arising from $Si(HPO_4)_2$ would be much weaked than the spinning sideband. No peak of P-OH groups of free phosphoric acid,

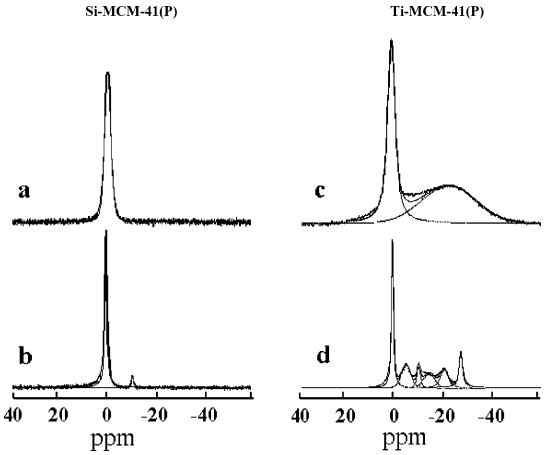

Figure 7. ^{31}P SPE (a and c) and SPE-MAS (b and d) NMR spectra and the corresponding fits of **Si-MCM-41(P)** (left) and **Ti-MCM-41-(P)** (right).

which normally appears in the 0.8−1.2 ppm region,[16] was observed.

Ti-MCM-41(P). The spectrum of **Ti-MCM-41(P)** (Figure 6d) is very similar to that of **Ti-MCM-41** (Figure 6c). It exhibits two resolved peaks: one at 2.1 ppm with a shoulder at 3.4 ppm and a weaker peak at 6.9 ppm. The peak at 2.1 ppm can be considered as a superposition of the peaks at 1.8 and 2.4 ppm, previously mentioned for **Ti-MCM-41**.

The shoulder at 3.4 ppm is most likely due to hydroxyls of phosphate groups as well as to residual water hydrogen-bonded to hydroxyls. The relative intensity of this peak (18%) is somewhat higher than in the spectrum of the initial **Ti-MCM-41** (12%) (Table 3). The relative intensity of the peak at 6.9 ppm is almost unchanged compared to **Ti-MCM-41** (6% and 5%, Table 3). This points toward the retention of the ═Ti(OH)-Si ═ groups upon modification with phosphate groups.

*3.3.2. ^{31} P SPE and SPE-MAS NMR. **Si-MCM-41(P)***. The ^{31}P SPE NMR spectrum of **Si-MCM-41(P)** (Figure 7a) shows a single peak at 0.1 ppm having a width at half-maximum ($\Delta\nu_{1/2}$) of 650 Hz (see also Table 4). This is attributed to H_3PO_4 covalently bonded to the surface.[17] In the SPE NMR (without MAS) results reported by Bogatyrev et al.,[17] the physically adsorbed orthophosphoric acid displays a considerably narrower peak with $\Delta\nu_{1/2}$ of 90 Hz. In addition to the single peak observed at 0.1 ppm ($\Delta\nu_{1/2}$ = 200 Hz) in the SPE spectrum, the ^{31}P SPE-MAS spectrum of **Si-MCM-41(P)** (Figure 7-c) includes another weak peak at −10.7 ppm ($\Delta\nu_{1/2}$ = 250 Hz). This suggests the existence of at least two types of chemically nonequivalent phosphorus atoms and, consequently, the formation of two types of silicon phosphate on the surface (species **1** and **2**, Table 4, Scheme 1). The relative intensity of the downfield peak (−10. 7 ppm) is ca. 6.5% (Table 4). By analogy with the results of Bogatyrev et al.,[17] where a similar peak was observed for phosphate-functionalized silica at −10.3 ppm, the peak at −10.7 ppm is attributed to condensed phosphates, e.g. silicon pyrophosphate (species **3**, Table 4).

Ti-MCM-41(P). The SPE and SPE-MAS spectra of **Ti-MCM-41(P)** are significantly different from those of **Si-MCM-41(P)**. The SPE spectrum (Figure 7-b) exhibits a relatively narrow peak at 0.4 ppm ($\Delta\nu_{1/2}$ = 700 Hz) of high intensity and a very broad one at −22.6 ppm ($\Delta\nu_{1/2}$ = 5000 Hz). In the SPE-MAS spectrum (Figure 7-d), the latter peak splits into five overlapping components (−5.4, −10.5, −14.7, −20.9, and −27.6 ppm) whereas the narrow peak is observed at 0.1 ppm. The whole spectrum was correctly fitted by a mixture of six Gaussian and lorenzian lines (Table 4).

The prevalence of the ≡Si−OH species on the surface of the starting Ti−MCM-41, as clearly shown by ^{1}H SPE-MAS NMR, suggests that the formation of silicon phosphate groups is favored. Consequently, we assign the strong peak to ≡SiO−$PO(OH)_2$ and $(\equiv SiO)_2$−PO(OH), as in **Si-MCM-41(P)**. The peak at −10.5 ppm (Figure 7c) most likely corresponds to silicon pyrophosphate, as in the spectrum of **Si-MCM-41(P)**.

The peaks at −5.4, −14.7, −20.9 and −27.6 ppm probably arise from titanium phosphate compounds (Table 4, species **4**−**7**). It was established that the ^{31}P chemical shifts of the titanium phosphates depend significantly on the preparation conditions and physical characteristics of the samples.[18] Moreover, there are significant divergences in the published data. Consequently, we cannot assign all the peaks precisely. However, by analyzing the most coherent data,[19,20] a tentative assignment was made by assuming the existence of titanium phosphate units such as (≡TiO)−$PO(OH)_2$ and $(\equiv TiO)_2$−PO(OH) covalently bonded to the surface, as well as titanium hydrophosphate $Ti(HPO_4)_2$ and titanium pyrophosphate TiP_2O_7. The latter structure cannot be covalently bonded to the surface and most probably exists in a quasi-amorphous state.

In this attribution, we also assumed that the replacement of the protons in phosphoric acid by the more electropositive titanium atoms induces an upfield shift of the corresponding peak. This upfield shift depends on the number of Ti atoms bonded to one phosphorus in the corresponding species.[18] Therefore, the peaks at −5.4 and −14.7 ppm may be assigned to the (≡TiO)−$PO(OH)_2$ and $(\equiv TiO)_2$−PO(OH) surface species, respectively (Figure 7-c, Table 4).

In the ^{31}P MAS NMR spectrum reported by Alfaya et al. on an amorphous material prepared by treating amorphous titanium-containing silica with phosphoric acid solution,[19] which is comparable to **Ti-MCM-41(P)**, a broad peak appears at about −8.3 ppm. Though the spectrum was not decomposed, we can assume that analogous chemical species, (≡TiO)−$PO(OH)_2$ (−5.4 ppm) and $(\equiv TiO)_2$−PO(OH) (−14.7 ppm), were formed.

The peak at −20.9 ppm (Figure 7c) can be reliably ascribed to structural $P(TiO)_3(OH)$ units of amorphous titanium hydrophosphate $Ti(HPO_4)_2 \cdot H_2O$, for which peaks at −18.4 or −19.3 ppm are reported.[19−21] It is noteworthy that the half-width of the ^{31}P peaks of these titanium phosphates is much greater than that of silicon phosphates (Table 4). This could imply greater chemical shift anisotropy of the phosphorus in titanium phosphates.

The last peak, at −27.6 ppm (Figure 7c), may be assigned to structural units of titanium pyrophosphate TiP_2O_7, reported to display a resonance at ca. −35 ppm.[19] Interestingly, this peak is much narrower than those (−5.4, −14.7, and −20.9 ppm) of the other titanium phosphates (Table 4). This narrowing is perhaps related to the different physical state of this species, which probably exists as an amorphous phase rather than as surface-grafted units.

Thus, ^{31}P NMR results reveal a variety of phosphate species (mixture of dihydrophosphate, hydrophosphate and pyrophosphate) on the surface of the phosphorylated **Si-MCM-41(P)** and **Ti-MCM-41(P)** samples. As far as can be judged on the basis of the ^{31}P NMR data, the chemical structure of the **Ti-MCM-41(P)** surface is similar to that of amorphous titanium-containing silica treated with a solution of phosphoric acid[19] and of mesoporous titanium phosphate obtained by template synthesis.[21] Furthermore, the phosphate composition of the **Ti-MCM-41(P)** surface differs from the known amorphous titanium phosphates prepared by precipitation and consisting mainly of hydrophosphate groups.

TABLE 4: Characteristics and Assignment of the Fitted Lines of the ^{31}P SPE (*) and SPE-MAS NMR Spectra of the MCM Samples[a]

samples	position (ppm)	rel intens (%)	width at half maximum (Hz)	assignment
***Si-MCM-41(P)**	0.1	100	650	≡SiO−PO(OH)$_2$ (**1**), (≡SiO)$_2$−PO(OH) (**2**)
Si-MCM-41(P)	0.1	94	200	≡SiO−PO(OH)$_2$ (**1**), (≡SiO)$_2$−PO(OH) (**2**)
	−10.7	6	250	≡SiO−PO(OH)−PO(OX)$_2$, X = H, Si≡ (**3**)
***Ti-MCM-41(P)**	0.4	83	700	≡SiO−PO(OH)2 (**1**), (≡SiO)-2-PO(OH) (**2**)
	−22.6	17	5000	
	0.1	57	250	≡SiO−PO(OH)$_2$ (**1**), (≡SiO)$_2$−PO(OH) (**2**)
	−5.4	9	900	≡TiO−PO(OH)$_2$ (dihydrophosphate) (**4**)
Ti-MCM-41(P)	−10.5	8	400	≡SiO−PO(OX)-PO(OX)$_2$, X = H, Si≡ (**3**)
	−14.7	5	1150	(≡TiO)$_2$═PO(OH) (hydrophosphate) (**5**)
	−20.9	7	750	Ti(HPO$_4$)$_2$ hydrophosphate (**6**)
	−27.6	14	300	TiP$_2$O$_7$ pyrophosphate (**7**)

[a] The numbers between parentheses in the assignment column correspond to the number of species shown in Scheme 1 and 2.

SCHEME 1. Species Grafted on Si-MCM-41(P) Surface

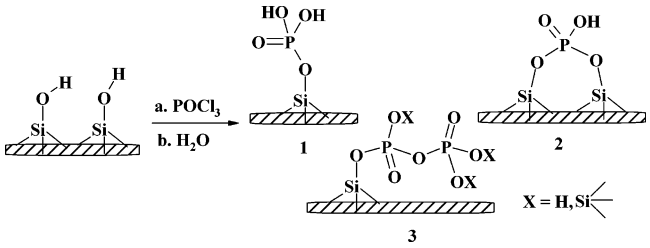

TABLE 5: Position and Assignment of the FTIR Bands of MCM Samples

samples	position (cm^{-1})	assignment
Si-MCM-41	960	ν (Si−OX), X = H, Ti, P
	800	ν (Si−O) Si−O−Si
Ti-MCM-41	965	ν (Si−OX), X = H, Ti, P
	790	ν (Si−O) Si−O−Si
Si-MCM-41(P)	970	ν (Si−OX), X = H, Ti, P
	800	ν (Si−O) Si−O−Si
Ti-MCM-41(P)	970	ν (Si−OX), X = H, Ti, P
	790	ν (Si−O) Si−O−Si

3.3.3. FTIR. The spectra of **Si-MCM-41**, of **Ti-MCM-41**, and of their phosphorylated derivatives are similar to those reported for precipitation silica, and show bands characteristic of silica lattice vibrations, Table 5.[22] Special attention was paid to the region of lattice vibration. The intensity of the band at 960 cm^{-1} due to ν (Si−O) in the ≡Si−OX group (X = H, M) is known to increase considerably upon replacement of the proton by metal atoms, e.g. Ti.[24,25] Indeed, this is observed in the spectrum of **Ti-MCM-41**. After the modification **Si-MCM-41** and **Ti-MCM-41** with phosphate groups, its maximum shifts to 970 cm^{-1}, and the relative intensity increases (Table 5). We suggest that this is related to the transformation of ≡SiO−H into ≡SiO−P bonds. The bands at 555 cm^{-1} ($TiO_{4/2}$ units in a titania matrix),[23] 670 and 785 cm^{-1} (characteristic of titanium silicates with high titanium content)[24,25] are not detected. The absorption of P═O[10] at 1050−1100 cm^{-1} is not observed either (spectra of **Si-MCM-41(P)**, **Ti-MCM-41(P)**), probably because of the strong silica lattice absorption in that region. However, a new broad band around 2300−2600 cm^{-1} is seen in the spectra of **Si-MCM-41(P)** and **Ti-MCM-41(P)**, and could be related to PO−H···H_2O adsorption.[26]

3.4. Acidic Properties. To estimate the number and the strength of acid sites in the functionalized samples, compared to the starting materials, desorption of adsorbed ammonia was studied by TPD (Figure 8 and Table 6).

Whereas the pure **Si-MCM-41**, activated at temperature T_a = 450 °C, is inactive in ammonia adsorption, **Ti-MCM-41** (T_a = 450 °C) exhibits acidic properties. The maximum ammonia desorption occurs at 210 °C. The concentration of the acid sites, calculated from this curve, is ca. 0.15 mmol g^{-1}. This low concentration indicates a small number of acidic bridged ≡Ti−(OH)−Si≡ groups, in agreement with the ^{1}H SPE-MAS NMR results (Table 3).

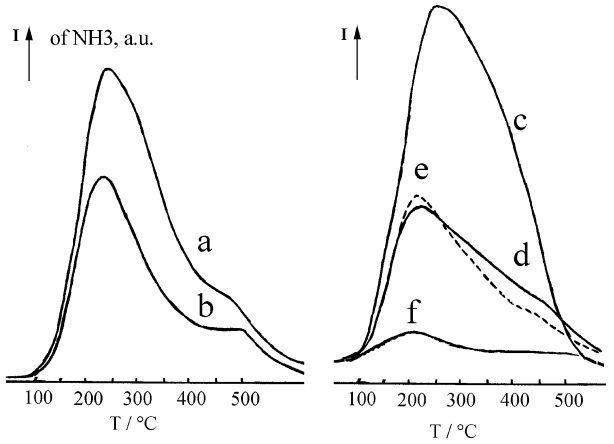

Figure 8. TPD curves of (a) **Si-MCM-41(P)** (T_a = 200 °C), (b) **Si-MCM-41(P)** (T_a = 450 °C), (c) **Ti-MCM-41(P)** (T_a = 200 °C), (d) **Ti-MCM-41(P)** (T_a = 450 °C), (e) **Ti-MCM-41(P)** (repeated desorption experiment on the sample, T_a = 450 °C), and (f) **Ti-MCM-41** (T_a = 450 °C). T_a is the activation temperature

TABLE 6: TPDA Data, Where T_a Is the Activation Temperature, N_a Is the Number of Acid Sites and T_{max} Is the Temperature Corresponding to the Maxima of Ammonia Desorption

samples	T_a (°C)	N_a (mmol g^{-1})	T^1_{max} (°C)	T^2_{max} (°C)	ref. to Figure 8
Ti-MCM-41	450	0.15	210		Figure 8f
Ti-MCM-41(P)	200	1.13	250	450	Figure 8c
	450	0.51	220	450	Figure 8d
	450[a]	0.48	215	450	Figure 8e
Si-MCM-41(P)	200	1.10	230	500	Figure 8a
	450[a]	0.74	230	500	Figure 8b

[a] Repeated measurement on the same sample after activation at 450 °C.

Si-MCM-41(P) and **Ti-MCM-41(P)**, activated at 200 °C, have considerably higher concentrations of acid sites. Indeed the values obtained are 1.10 mmol g^{-1} for **Si-MCM-41(P)** and 1.13 mmol g^{-1} for **Ti-MCM-41(P)**. After activation at 450 °C the number of acid sites is reduced to 0.74 mmol g^{-1} for the former and to 0.51 mmol g^{-1} for the latter. This reduction with the increase in T_a is due to dehydroxylation of the grafted acid (thermogravimetry results, Figure 5) followed by the formation of pyrophosphate. Once formed, these species are stable, so that a repeated thermal activation and NH_3 adsorption on **Ti-MCM-**

SCHEME 2. Species Grafted on Ti-MCM-41(P) Surface

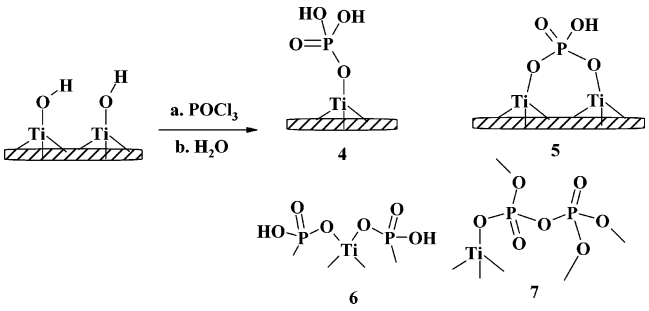

41(P) give approximately the same value, 0.48 mmol g^{-1} (Figure 8e and Table 6).

For **Si-MCM-41(P)** and **Ti-MCM-41(P)**, two desorption maxima are observed (Figure 8, parts a and c, see also Table 6). The first maximum occurs at $T^1_{max} = 230$ °C for **Si-MCM-41(P)** and $T^1_{max} = 250$ °C for **Ti-MCM-41(P)** and the second at $T^2_{max} = 500$ °C for the former and $T^2_{max} = 450$ °C for the latter. This result reveals the existence of two types of acid sites with two different acidities: moderate (first desorption maxima) and stronger acidity (second desorption maxima), which are due to different P−OH groups in the different phosphate structures. It is worth noting that the phosphate concentration on **Si-MCM-41(P)** (ca. 1.0 mmol g^{-1}) corresponds approximately to the number of acid sites, calculated from TPD (1.10 mmol g^{-1}). Thus, it can be deduced that the modification of silica with phosphate groups affords mainly bidentately grafted phosphate species providing one acid site per phosphate unit as illustrated in Scheme 1, species **2**. Concerning **Ti-MCM-41(P)**, despite the 2-fold greater phosphate concentration (ca. 2.2 mmol g^{-1}), the number of acid sites is 1.13 mmol g^{-1} (Table 6). This suggests that the majority of the phosphate units are bonded in nonacidic titanium phosphates, e.g. titanium pyrophosphate (Scheme 2, species **7**). As discussed above, the increase in the activation temperature from 200 to 450 °C results in a 2-fold decrease in the number of acid sites, while both types of acid sites (moderate and strong) continue to coexist (Figure 8).

4. Discussion and Conclusion

The TPD and the ^{1}H SPE-MAS NMR results have shown the absence of acidic properties in a purely siliceous sample (starting **Si-MCM-41**) and the existence of strong acid sites (0.15 mmol g^{-1}) in **Ti-MCM-41**. As suggested by the ^{1}H SPE-MAS NMR results, these sites are the bridging hydroxyls in ≡Si−(OH)−Ti≡ species.

Modification with phosphate groups of both **Si-MCM-41** and **Ti-MCM-41** materials creates new acid sites (of moderate and stronger acidity, according to the TPD results) while, to a certain degree, the initial structural characteristics (high surface area, narrow pore size distribution, and crystalline hexagonal structure) are preserved. Thus, **Si-MCM-41(P)** has 1.10 mmol g^{-1} of acid sites (Table 6) in combination with good structural characteristics (surface area 819 m^2 g^{-1}, pore volume 0.595 cm^3 g^{-1}). Modification of **Ti-MCM-41** with phosphate groups results in a similar increase in the number of acid sites (1.13 mmol g^{-1}, TPD), but with poorer structural parameters, namely surface area (510 m^2 g^{-1}) and pore volume (0.221 cm^3 g^{-1}) (Table 2).

NMR results show that the surface of phosphate-functionalized materials contains a variety of phosphate species, described below (Schemes 1 and 2), as well as other functional groups including unreacted silanols and ≡Si−(OH)−Ti≡ species (**Ti-MCM-41(P)**).

Modification of **Si-MCM-41** with $POCl_3$ followed by hydrolysis of P−Cl bonds is illustrated in Scheme 1. According to the ^{31}P NMR data (Table 4), the **Si-MCM-41(P)** surface contains grafted species **1** [dihydrophosphate ≡SiO−$PO(OH)_2$], **2** [hydrophosphate $(=SiO)_2$−PO(OH)], and **3** [pyrophosphate, e.g. ≡SiO−PO(OH)−PO(OH)-OSi≡].

Dihydrophosphate and hydrophosphate species represent ca. 94% of all grafted phosphates. The ratio (∼1/1) of the concentration of phosphate groups (elemental analysis) to the acid sites (TPD, Table 6) suggests that the one-proton hydrophosphate species **2** are the most favored. The silicon pyrophosphate (species **3)** constitutes ca. 6% of the grafted phosphate groups. ^{1}H SPE-MAS NMR results on **Si-MCM-41(P)** and **Ti-MCM-41(P)** show that hydroxyl groups of the grafted acid make up ca. 20% of the surface hydroxyls.

With regards to these results, it is important to mention that both mono- and bi-dentate bonding of phosphorus-containing units to silanols is claimed.[10,17] Thus, the interaction of PCl_3 with aerosil results in =Si−O−PCl_2 groups.[17] Similarly, the interaction of $POCl_3$ and PCl_3 with SiO_2 and Al_2O_3 as well as alumosilicates proceeded via monofunctional binding of both reagents to hydroxyls. In the latter case the formation of a silicon pyrophosphate type species is predominant, as previously reported.[27]

Dehydroxylated pyrogenic silica has an average distance between isolated silanols of 5−7 Å, which argues in favor of monofunctional binding,[28] whereas an average distance between neighboring silanol groups on the surface of MCM-41 is ca. 5 Å.[29] In this case, bifunctional linkage of $POCl_3$ with the surface may become more probable (Scheme 1, species **2**).

Modification of **Ti-MCM-41** with phosphate groups results in a considerable increase in the acid site number (1.13 mmol g^{-1}) and worsening of its structural parameters, such as surface area and pore volume (Table 2). A number of phosphate-containing species are formed on its surface (Scheme 2), first of all the silicon phosphates **1**−**3** (Scheme 1), similar to what is observed for **Si-MCM-41(P)**. Species **1** prevails (57%, Table 4). There is slightly more of species **3** (Table 4, 8% or 12% of the total silicon phosphates) than on the **Si-MCM-41(P)** surface (6%). Titanium-bonded species (Scheme 2): surface-grafted titanium dihydrophosphate (≡TiO)-$PO(OH)_2$ (**4**), surface-grafted titanium dihydrophosphate $(=TiO)_2$−PO(OH) (**5**), titanium hydrophosphate $Ti(HPO_4)_2$ (**6**), and titanium pyrophosphate TiP_2O_7 (**7**) are present in a ratio 1.8/1.0/1.4/2.8 (calculated from Table 4, ^{31}P MAS NMR). Species **4** and **5** are attached to the surface by −TiO− linkages, whereas **6** and **7** probably build up an amorphous phase on the surface (as shown by TEM). Their formation involves the cleavage of Si−O−Ti and Ti−O−Ti bonds and may result in partial etching of the surface.

As shown in Schemes 1 and 2, most of the grafted species (species **1**−**6**) contain acidic protons (ca. 1.1 mmol g^{-1}). Treatment at 450 °C reduces the number of acid sites (to ca. 0.51−0.74 mmol g^{-1}) as a result of the condensation of grafted phosphates and the formation of pyrophosphates.[19] Interestingly, **Ti-MCM-41(P)** and **Si-MCM-41(P)** have the same number of acid sites (ca. 1.1 mmol g^{-1}, TPD Table 6), despite the higher phosphate concentration in the former (2.2 and 1.0 mmol g^{-1}, respectively). This suggests that the acidity of both samples, **Si-MCM-41(P)** and **Ti-MCM-41(P)**, is mainly due to the grafted silicon hydro- and dihydrophosphate species.

In conclusion, modification of **Si-MCM-41** and **Ti-MCM-41** with $POCl_3$ afforded materials with a mesoporous framework and an acidic surface functionalized with silicon and titanium phosphate species. Our preliminary tests on esterification

catalysis show future perspectives of these materials as solid acid catalysts.

Acknowledgment. The authors thank INTAS (Grant 97/1116) and NATO (Grant SfP-97/1896) for financial support.

References and Notes

(1) Kresge, C. T.; Leonowicz, M. E.; Roth, W. J.; Vartuli, J. C.; Beck J. S. *Nature (London)* **1992**, *359*, 710.
(2) Yue, Y.; Gedeon, A.; Bonardet, J. L.; Melosh, N.; d'Espinose, J. B.; Fraissard, J. *Chem. Commun.* **1999**, *19*, 1967.
(3) Berlini, C.; Guidotti, M.; Moretti, G.; Psaro, R.; Ravasio, N. *Catal. Today* **2000**, *60*, 219.
(4) Neumann, R.; Levin-Elad, M. *J. Catal.* **1997**, *166*, 206.
(5) Kovalenko, A. S.; Ilin, V. G.; Filippov, A. P. *Theor., & Exp. Chem.* **2000**, *36*, 322.
(6) Marchese, L.; Gianotti, E.; Maschmeyer, T.; Martra, G.; Coluccia, S.; Thomas, J. M. *Nuovo Cimento Soc. Ital. Fis. D-Condens. Matter At. Mol. Chem. Phys. Fluids Plasmas Biophys.* **1997**, *19*, 1707.
(7) Chiker, F.; Nogier, J. P.; Launay, F.; Bonardet, J. L. *Appl. Catal., A* **2004**, *259*, 153.
(8) Maschmeyer, T.; Rey, F.; Sankar, G.; Thomas, J. N. T. *Nature (London)* **1995**, *378*, 159.
(9) Kovalenko, S.; Korchev, A. S.; Chernenko, V. *Adsorpt. Sci. Technol.* **1999**, *17*, 245.
(10) Golub, A.; Sevastyanova, O. B.; Korchev, A. S.; Pavlov, D. O. *Ukr. J. Chem.* **1996**, *62*, 73.
(11) Iler, R. *The Chemistry of Silica;* Wiley: New York, 1971, p 562.
(12) Nekrasov, B. V. *Comprehensive Inorganic Chemistry* (in Russian); Khimija: Moscow, 1974.
(13) Enriquez, M. A.; Doremieux-Morin, C.; Fraissard, J. *J. Solid State Chem.* **1981**, *40*, 233.
(14) Mastikhin, V. M.; Mudrakovsky, I. L.; Nosov, A. V. *Prog. NMR Spectrosc.* **1991**, *23*, 259.
(15) *The Surface Properties of Silicas*; Legrand, A., Ed.; J. Wiley and Sons Ltd.: London, 1998.
(16) Zahedi-Niaki, M. H.; Laidi, S. M. L.; Kaliaguine, S. *Microporous Mesoporous Mater.* **1999**, *32*, 252.
(17) Bogatyrev, V. M.; Brei, V. V.; Chuiko, A. A. *Theor. Exp. Chem.* **1988**, *24*, 629.
(18) Randarevitch, S. B.; Strelko, V. V.; Beljakov, V. N. *Theor. Exp. Chem.* **1988**, *24*, 633.
(19) Alfaya, A. A. S.; Gushikem, Y.; de Castro, S. C. *Chem. Mater.* **1998**, *10*, 909.
(20) Roca, S.; Airoldi, C. *Thermochim. Acta* **1996**, *284*, 289.
(21) Bhaumik, A.; Inagaki, S. *J. Am. Chem. Soc.* **2001**, *123*, 691.
(22) Hair, M. *Infrared Spectroscopy in Surface Chemistry*; M. Dekker Inc.: New York, 1967.
(23) Vasylov, G. N. *Catal. Rev.* **1997**, *39*, 209.
(24) Astorino, E.; Peri, J. B.; Willey, R. J.; Busca, G. *J. Catal.* **1995**, *157*, 482.
(25) Alba, M. A.; Luan, Z.; Klinowski, J. *J. Phys. Chem.* **1996**, *100*, 2178. Chen, L. Y.; Jaenicke, S.; Chuan, G. K. *Micropor. Mater.* **1977**, *12*, 323. Hitz, S.; Prins, R. *J. Catal.* **1997**, *168*, 194; Fejes, P.; B'Nagy, J.; Kovács, K.; Vankó, G. *Appl. Catal., A: Gen.* **1996**, *145*, 155.
(26) Gordon, A.; Ford, P. *Sputnik Khimika* (in Russian); Rosenberg, E. L., Ed.; Mir: Moscow, 1976.
(27) Pawxula, M.; Marczewski, M. Krzywicki, A. *Proc. Vth Inter. Symp. Heterogeneous Catal., Varna*, **1983**, *Part II*, 285.
(28) *Chemistry of the Silica Surface*, Chuiko, A. A., Ed.; Kiev, 2001.
(29) Mercier, L.; Pinnavaia, T. J. *Adv. Mater.* **199**, *9*, 500.